Self-matched high-Q reconfigurable antenna concept for mobile terminals

Bahramzy, Pevand; Jagielski, Ole; Svendsen, Simon; Pedersen, Gert Frølund

Published in:
IET Science, Measurement & Technology

DOI (link to publication from Publisher):
10.1049/iet-smt.2014.0013

Publication date:
2014

Document Version
Publisher's PDF, also known as Version of record

Published in IET Science, Measurement and Technology
Received on 8th January 2014
Revised on 6th April 2014
Accepted on 24th April 2014
doi: 10.1049/iet-smt.2014.0013

ISSN 1751-8822

Self-matched high-*Q* reconfigurable antenna concept for mobile terminals

Pevand Bahramzy[1,2], *Ole Jagielski*[1], *Simon Svendsen*[1], *Gert F. Pedersen*[2]

[1]*Intel Mobile Communication Denmark Aps, Norresundby, Denmark*
[2]*Section of Antennas, Propagation and Radio Networking (APNet), Aalborg University, DK-9220 Aalborg, Denmark*
E-mail: pevand.bahramzy@intel.com

Abstract: This study presents reconfigurable antenna design for a front end (FE) that has separate transmit (Tx) and receive (Rx) path. In such an FE, the Tx and Rx antennas can be content with covering only the transmit and receive channels in a frequency band. Therefore they can be quite narrow-band. Narrow-band antennas can exhibit high losses, because of the relative high current density per area and limited tuning/matching component *Q*. To address this, a self-matched antenna design is introduced, having the tunable capacitor as the only physical component. The Tx and Rx narrow-band antennas are designed to cover the frequency range 1710–2170 MHz. Metrics as for example, impedance bandwidth and efficiency are obtained both in simulations and measurements.

1 Introduction

Owing to the cellular technology evolution (GSM, UMTS, LTE) modern mobile handsets are required to operate at multiple frequency bands to provide enhanced and multifunctional performances. Owing to the many supported frequency bands and multimode operations [1], the radio frequency (RF) front end (FE) is complicated a lot. Moreover, there is a trend towards highly integrated devices that are slimmer and lighter with very limited printed circuit board (PCB) area available for antennas. Conventional passive multiband antennas require large antenna volume [2–6]. Thus, covering a single very wide frequency band or multiple frequency bands, while maintaining small size and high efficiency, is a major challenge because of limitations by fundamental relationships between antenna size, bandwidth and efficiency [7].

Wideband coverage issue can be addressed through the use of tunable antennas with frequency selectivity. With this approach the antenna can be downsized, whilst increasing the bandwidth trough tunability. In addition, the antenna tuning can be used to compensate for proximity effects occurring because of the user or changes in the operating environment.

The problem of a complicated RF FE, because of the increasing number of bands and band combinations, may be overcome through co-design with the antenna system, which can help miniaturising the antenna and the FE, while covering the increased number of bands. Such an approach is proposed to have separate transmitter (Tx) and receiver (Rx) path throughout the FE [8–10], thus requiring separate Tx and Rx antennas. Since these two antennas need to cover only the transmit and receive channels in a band, they can be quite narrow band. The space occupied by the antennas is greatly reduced as the same elements are used to cover all the bands. Furthermore, these antennas are designed for their highest targeted band of operation which result in small size elements [7]. High isolation can be obtained between Tx and Rx antennas because of the narrow-band characteristic and frequency offset, providing filtering. Hence, part of the required isolation can be provided by the narrow-band antennas and part of it by the tunable filters. An isolation of some 25 dB is required to be provided by the antennas [11].

FE architecture with separate Tx and Rx tunable narrow-band antennas was first conceptualised in 2003 [12], and since then several investigations have been carried out on this concept. Some papers have mainly addressed the isolation issue between the Tx and Rx antennas. In [8, 13] it is proposed to improve the isolation by introducing a spatial filter, where the spatial filter is synthesised by equipping the Tx with at least one more antenna than the Rx, resulting in a balanced Tx antenna and unbalanced Rx antenna. Isolation study of wide-band, medium-band and narrow-band antennas is conducted in [9, 14] to show the advantage of narrow-band antennas in terms of isolation. The challenges of frequency tunable high-*Q* antennas have been discussed in [15–17]. An investigation on currents running through the source, the short and the capacitor of a tunable planar inverted F antenna for hand-held devices, has been performed in [15]. The loss mechanism of tunable high-*Q* antennas is investigated in [16] and proposes a distributed tuning mechanism in order to reduce the loss because of the tuning component. The work in [17] highlights the efficiency issue of a tunable high-*Q* antenna by comparing it with a low-*Q* antenna. The effect of user on tunable high-*Q* antennas is studied in [9, 18], where

low-Q and high-Q antennas are compared with respect to detuning in frequency, absorption loss and mismatch loss. Tunable Tx and Rx antennas, using RF micro-electro-mechanical systems (MEMS) tunable capacitor, are presented in [19], where the tunable capacitor is mounted at the open end of traditional inverted F antenna. None of these papers have proposed an optimal and new antenna concept tailored for the FE with separate Tx and Rx antennas.

As addressed in [15–17], there are some conceivable drawbacks of frequency tunable high quality factor (Q) antennas, which among other things are because of relative high current density on the antenna structure and limited tuning/matching component Q. Hence, the active antennas can exhibit high RF power loss, poor linearity and high dc power consumption. Moreover, higher maximum rating requirements for the tuning components become crucial.

Owing to the inherently high current density, High-Q antennas are more challenging to work with. Therefore, in this paper, special focus is on each of the loss contributors (conductor, antenna carrier and tuning/matching components) to find new optimal solutions for the high-Q frequency agile antennas. The antenna structure design is done for less sensitiveness against the high current density. As few as possible tuning/matching components are used in order to reduce the losses caused by these components. In addition, matching components are integrated in the antenna structure in order to achieve highest possible component Q, leading to self-matched antenna. The dielectric losses from the antenna carrier are reduced by avoiding placement of the carrier at the inner surface of the radiator, where high E-fields typically exist.

Frequency tunability for handset applications has been proposed with various switching techniques such as RF switches, MEMS switches, PIN diodes and varactors [20–30]. In this paper, RF MEMS capacitors are used as tuning components because of their high-Q and high linearity performance. LTE band I, II and III (1710–2170 MHz) are selected for the proof of concept before going to the more challenging bands below 1 GHz.

Section 2 of this paper introduces the antenna concept and the design improvement is explained in Section 3. Following this in Section 4 the measured impedances and total efficiencies of the improved design are presented. Finally, conclusion is given in Section 5.

2 Antenna design

Fig. 1 depicts the geometry of the proposed antenna concept, which is applied for the Tx and Rx operation through separate radiators. The structure incorporates an antenna element, feeding with matching components, a coupler and a tuning capacitor connected to it. The Tx and Rx antennas have total volume of $L \times W \times H = 9 \times 8 \times 4$ mm^3 and $9 \times 6 \times 4$ mm^3, respectively. The Rx antenna is slightly smaller because of operation at higher frequencies. The antennas are mounted on a $120 \times 55 \times 1$ mm^3 PCB with no ground clearance.

As illustrated in Fig. 2, the element is connected to PCB through feed and matching components and the coupler is connected through tuning capacitor C_t. The coupling capacitor C_c, shown in Fig. 1, is the capacitive connection between the element and the coupler. The unmatched impedance of one of the antennas is shown in Fig. 3. The impedance match is then obtained through L_s and L_p

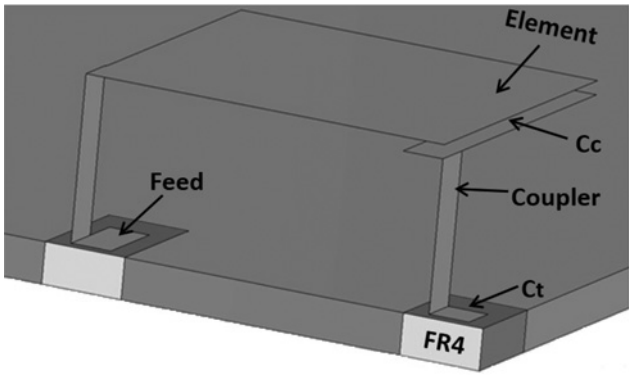

Fig. 1 *Antenna geometry*

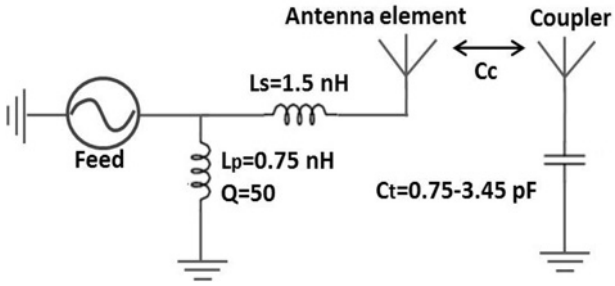

Fig. 2 *Circuit diagram of the antenna system*

matching inductors. The element is capacitively coupled to the coupler through coupling capacitor C_c, resulting in capacitive loading. The capacitor C_c is built in the antenna structure with 0.3 mm separation distance between the element and the coupler, where air is used as the dielectric to obtain high Q. The electrical length of the antenna is altered by varying the value of C_t with a step size of 125 fF. The LTE bands I–III can be covered by varying the capacitance of C_t.

High AC voltage across the tuning capacitor of tunable antennas is a typical problem and therefore taken into consideration in the design phase.

High isolation between the Tx and Rx antennas is crucial utilising the proposed FE architecture. Hence, a parameter study of antennas positions on the PCB is performed in search of optimal isolation. As illustrated in Fig. 4, four antenna position configurations have been analysed. In configurations (a) and (b) both antennas are located at the top with different feed and tuning capacitor positions. The

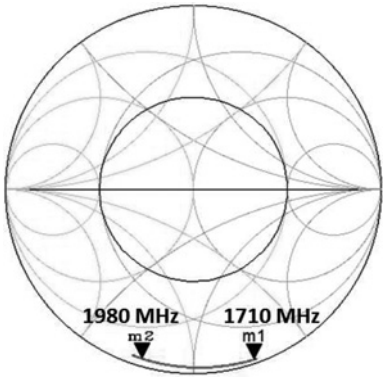

Fig. 3 *Tx antenna unmatched impedance*

doi: 10.1049/iet-smt.2014.0013

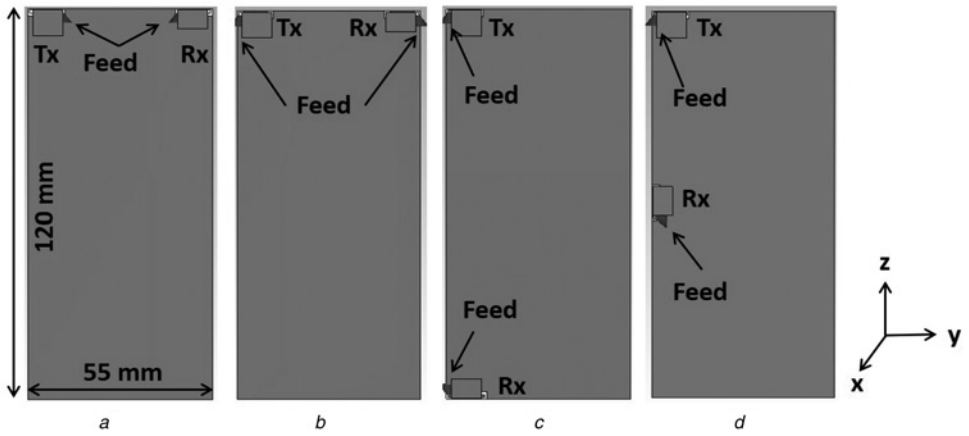

Fig. 4 *Different position scenarios on the PCB*

a Tx and Rx at top with feed 10 mm away from each edge
b Tx and Rx at top with feed at each edge
c Tx at top and Rx at bottom with corner feed
d Tx at top and Rx at side

classical top and bottom antenna positions are considered in (c), whereas (d) covers the recent used top and side positions.

2.1 Simulation results

The geometrical dimensions and the values of the components are obtained by using the EM software CST Microwave Studio [31] and ADS [32], respectively.

2.1.1 Results of antenna position scenarios on the PCB: The simulated reflection coefficients of different antennas positions on the PCB are shown in Fig. 5. From the figure it can be seen that the Tx antenna has smaller bandwidth in (a), where the feed is located 10 mm from the corner of the PCB. In the remaining three configurations, the Tx feed is placed at the corner of the short side and therefore excites the PCB mode better, resulting in more bandwidth. For the same reason the Rx antenna exhibits more bandwidth in (b) and (c), whereas in positions (a) and (d) the bandwidths are smaller.

Worst case isolation is defined as the maximum value of S_{21} in dB over the frequency range corresponding to a particular bandwidth. Fig. 6 presents the worst case isolation results at LTE bands I, II and III, where it can be observed that configurations (a) and (c) show isolation of some −25 dB or better, whereas (d) exhibits slightly worse isolation with (b) being the worst (−13 dB). Placement of the antennas, in (a), are optimised for best isolation compromising the bandwidth. The higher isolation in (a), compared to (b), is because of the narrower bandwidth (see Fig. 5) caused by the feed points being 10 mm away from the corner of the PCB. Configuration (c) shows highest isolation simply because of largest distance, and as Rx antenna is moved closer to the Tx antenna (configuration (d)), the isolation starts degrading. Configurations (a) and (c) both provide the required

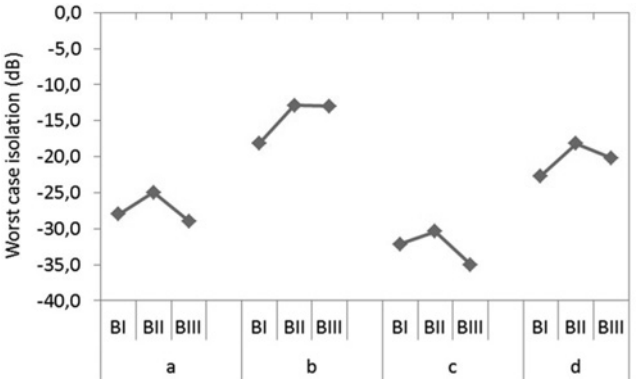

Fig. 6 *Simulated worst case coupling coefficients (S_{21}) for the different position configurations at LTE Band I, II and III*

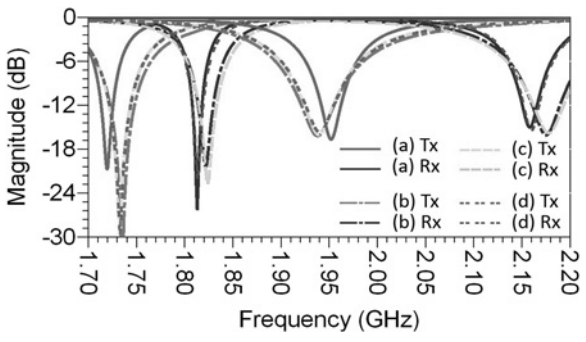

Fig. 5 *Simulated reflection coefficients of Tx and Rx antennas for the different position configurations, tuned at highest and lowest operating frequencies*

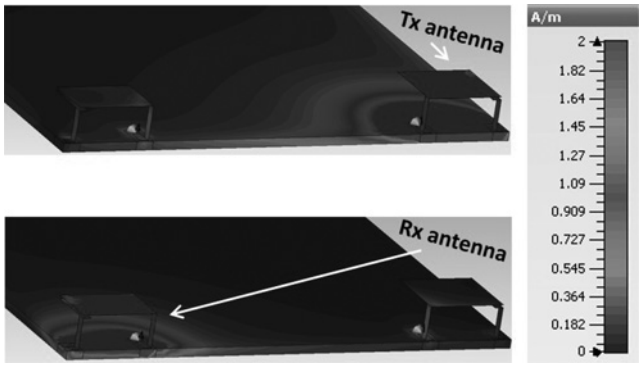

Fig. 7 *Current distribution: Tx antenna at 1955 MHz and Rx antenna at 2160 MHz*

isolation (25 dB). Therefore throughout the paper one of these two position scenarios is chosen for investigations, which is configuration (a).

2.1.2 Results based on configuration (a): The current distribution plots are shown in Fig. 7, which show how coupled the two antennas are. With the Tx antenna operating at 1955 MHz (top plot in the figure) minimum amount of currents can be observed at the opposite end of PCB, where Rx antenna is located. The same is the case for the bottom plot, where Rx is operating at 2160 MHz.

The simulated scattering parameters and impedances, at different values of C_t, are shown in Fig. 8. As C_t of each antenna is varied, tuning is obtained over a wide frequency range: 1710–1980 MHz for the Tx antenna and 1805–2170 for the Rx antenna. The figure shows only the scattering parameters and impedances with correct duplex spacing between the Tx and the Rx antennas. With C_t set to the smallest value (C_{min}), the antennas resonate at highest frequency of operation. As C_t increases the resonances tune down in frequency with finally resonating at lowest operation frequency for C_t set to maximum value (C_{max}). The maximum and minimum bandwidth, for the Tx and Rx antennas at SWR = 3, are 53–24 and 48–23 MHz, respectively.

As illustrated in Fig. 1, capacitive loading is achieved by placing the coupler at open-end of the element where high *E*-field exists and therefore causes highest capacitive load, forcing the antenna resonance down to the frequency of interest. Another advantage of placing the coupler at open-end is that very stable impedance is obtained as tuning the antenna impedance.

The coupling capacitor C_c and tuning capacitor C_t form series connection, leading to voltage division. The total capacitance is given by $C_{total} = q/V_{total}$, where q is the amount of charge stored and V_{total} is the voltage split into V_t and V_c. Hence, $1/C_{total} = 1/C_t + 1/C_c$. From the formulas it is observed that the capacitors voltage divides in inverse proportion to the ratio of their capacitance, meaning that the capacitor with twice the capacitance of the other will have only half the voltage of the other. The peak AC voltage across capacitors C_c and C_t, with 30 dBm input power (GSM), is illustrated in Fig. 9. As observed in the figure, the voltage across the variable capacitor C_t decreases whereas it increases across the fixed capacitor C_c, as tuning down in frequency.

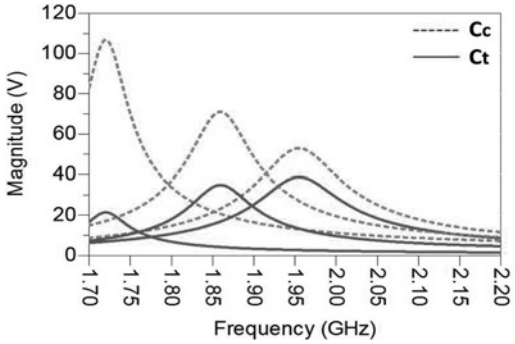

Fig. 9 *Simulated peak voltage across the Tx antenna tuning capacitor C_t and coupling capacitor C_c with 30 dBm input power*

Because of the series combination, C_{total} is mostly affected by the smaller capacitor C_c. Furthermore, the tuning resolution is controlled by adjusting the value of C_c, which is a very important feature of this concept since any desired tuning resolution can be achieved without the need for changing the position of C_t, as is the case for tuning conventional antenna concepts [17, 33]. Decreasing C_c causes higher tuning resolution, but larger C_t tuning range is required in return to tune down to the lowest operation frequency. Hence, tuning resolution is adjusted at the highest frequency of operation, where tuning resolution is coarse, to achieve the requisite SWR = 3 match tuning resolution and obtain relatively small C_{max} within the tuning range of the variable capacitor.

For mobile devices, used in multipath environment and varying orientations, total efficiency becomes an important figure of merit. In addition, efficiency deterioration caused

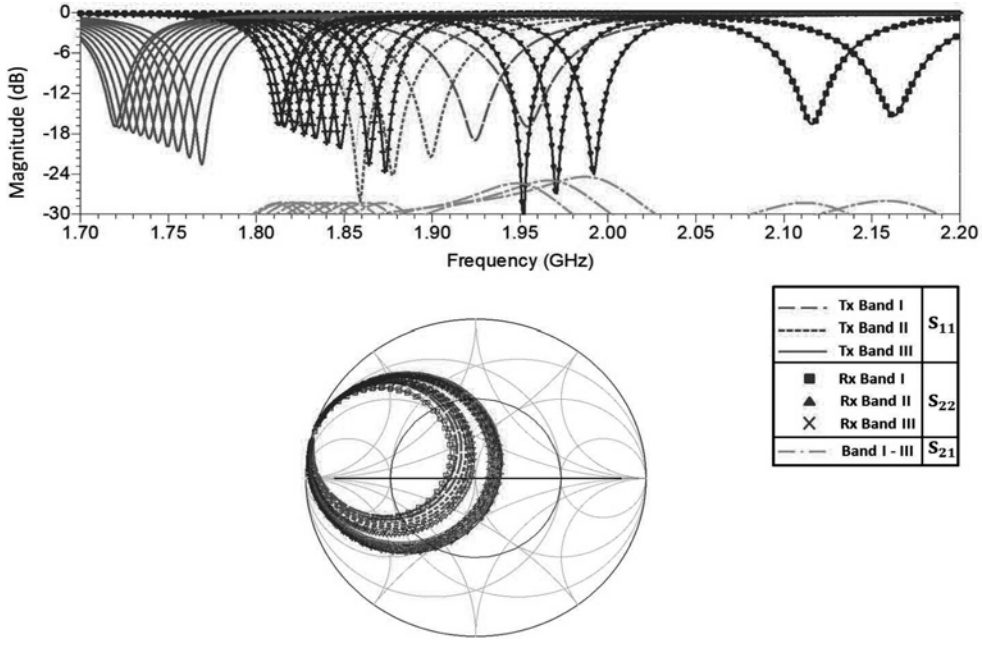

Fig. 8 *Simulated scattering parameters and impedances*

Reflection coefficients (S_{11}, S_{22}) and coupling coefficient (S_{21}) of the Tx and Rx antennas tuned in the three LTE frequency bands together with matched impedances in the smith chart

doi: 10.1049/iet-smt.2014.0013

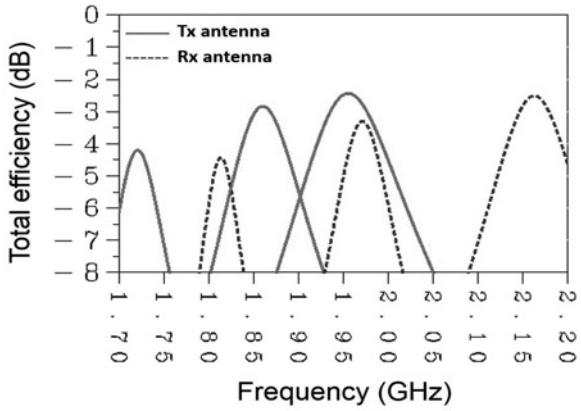

Fig. 10 *Simulated FS total efficiency of Tx and Rx antennas with varying tunable capacitor Q*

by the tuning components is one of the major drawbacks of tunable antennas. Hence, the simulated free space (FS) total efficiencies of the Tx and Rx antennas, at three different tuning states, are presented in Fig. 10. Owing to the inverse relationship of C_t value and its Q ($Q = 1/\omega CR$), the results are shown for C_t Q varying from 70 to 40 and C_t value varying between 0.75 and 3.45 pF. C_t Q is set to 70 at highest frequency of operation and 40 at lowest frequency of operation. The peak efficiencies vary between −2.4 and −4.3 dB for Tx antenna and between −2.5 and −4.5 dB for Rx antenna.

3 Design improvement

To follow up on the design guidelines, for designing efficient high-Q antennas, given in the introduction, it is investigated here how the amount of matching components can be reduced. Since C_c already has high Q and C_t has fixed Q provided by the supplier, the only possible way to improve the efficiency is by improving the matching circuit Q. This is resolved by replacing the matching inductors L_s and L_p. The series inductor L_s used in the matching circuit can be omitted by creating an open stub in the element, as depicted in Fig. 11. The open stub represents a parallel capacitor seen from the stub itself. However, the phase shift from the feed to the stub transforms the parallel capacitor to a series inductor, replacing the inductor L_s from the matching circuit. The value of L_s can be controlled by adjusting the stub length.

To further improve the matching circuit Q, the parallel inductor L_p is replaced by a closed slot with the feed fed across it, where the element itself is shorted to ground (see Fig. 11). Hence, the slot in the PCB acts as the inductor L_p.

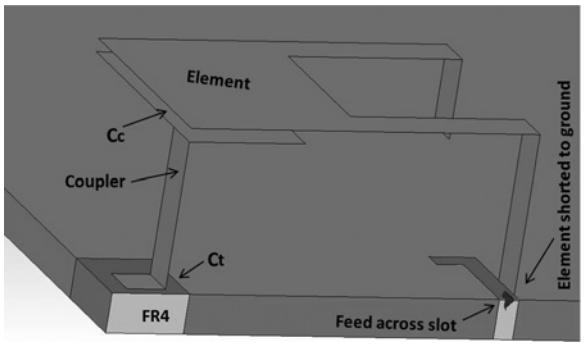

Fig. 11 *Geometry of the self-matched antenna design*

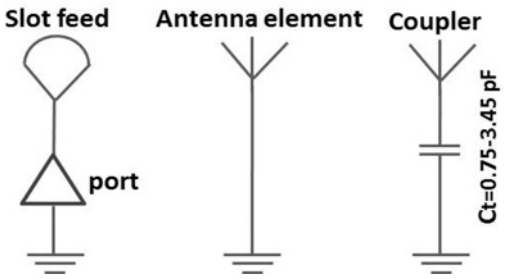

Fig. 12 *Circuit diagram of the self-matched antenna design*

Table 1 Simulated FS total efficiency of the improved antenna design

	f_r, MHz	C_t, pF	Q_{C_t}	η_T, dB
Tx	1966	0.75	70	−2.0
	1868	1.25	64	−2.2
	1723	3.45	40	−3.4
Rx	2157	0.75	70	−2.3
	1967	1.50	61	−2.7
	1813	3.45	40	−3.7

The circuit diagram of this improved design is depicted in Fig. 12, where it is seen that now there is no physical matching components there, resulting in improved total antenna Q. After omitting the physical matching components, C_t is the only requisite physical component, resulting in self-matched antenna concept.

By applying the slot feeding technique, the robustness against electrostatic discharge (ESD) also increases, because the antenna element is shorted to ground instead of connected to a feed point. In addition, the tuning component C_t is less exposed to ESD because it is not directly connected to the element. This leads to an antenna design with less sensitiveness against ESD. Owing to this the requirement for external circuits for ESD protection can either be relaxed or removed completely.

The efficiency results of the improved antenna design are depicted in Table 1. The results are shown at three different tuning frequencies with varying C_t Q. The Tx and Rx antennas peak efficiency vary from −2.0 to −3.4 dB and from −2.3 to −3.7 dB, respectively. Improvement at lowest frequencies of operation is around 1 dB, whereas at highest frequencies of operation the improvement is lesser because of lower antenna Q.

4 Measurement results

In order to verify the performance of the antenna, a prototype is fabricated and measured. A PCB is specifically designed and fabricated for this purpose. The PCB with mounted antennas is presented in Fig. 13. The MEMS tunable digital capacitor array (TDCA), provided by Wispry [34], is used as the tunable capacitor for tuning the antennas. The used TDCA provides a total capacitance of $C_{min} \simeq 0.75$ pF – $C_{max} \simeq 4.5$ pF, has a step size of 125 fF and is able to handle RMS RF voltage of up to 40 V, corresponding to peak voltage close to 57 V, which is sufficient for the proposed antenna concept (see Fig. 9). It needs biasing voltage of 3.3 V and is controlled through serial peripheral interface line commands.

For optimised performance, the layout of antenna and TDCA must be designed in such a way that they are closely

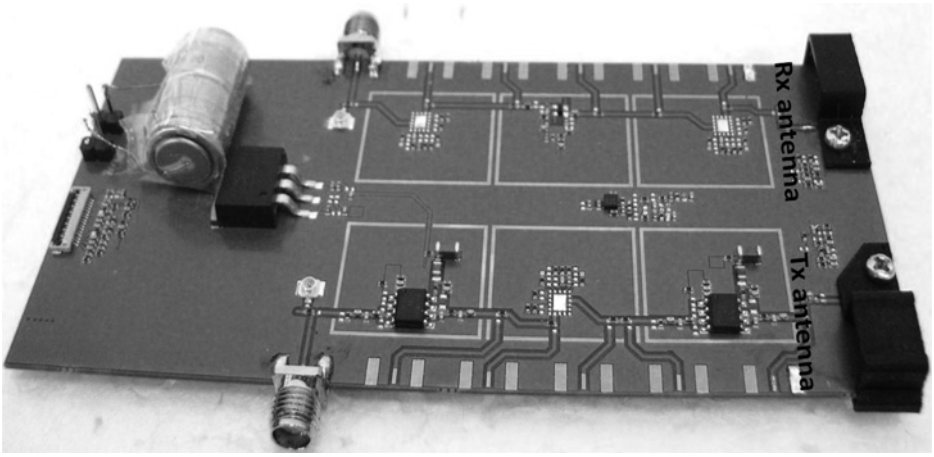

Fig. 13 *PCB with mounted antennas*

connected. Therefore the TDCA is placed beneath the antenna structure with <1 mm micro-strip line to the coupler connection pad (See Fig. 14*a*). An investigation is carried out to ensure that the high electric fields from the antenna do not damage or detune the TDCA. In Fig. 15 it is observed that the electric fields are much stronger in the gap between the coupler and the element (C_c) than between the coupler/element and PCB. Furthermore, the peak voltage across C_c is 108 V at 1723 MHz (see Fig. 9), which results in electric field of around 108 V/0.3 mm = 360 000 V/m. The peak voltage in TDCA from [34] is 57 V. Assuming 5 µm separation distance in the TDCA gives electric field of around 57 V/5 µm = 11 400 000 V/m. The peak RF voltage in the TDCA is roughly 11 400 000/360 000 = 31 times larger. Hence, it is expected to function as intended under the antenna structure.

Placing a carrier at the inner surface of the antenna structure will subject it to high electric fields, leading to high dielectric loss. In order to minimise the dielectric loss, caused by the carrier, the carrier is mounted at the outer surface of the antenna structure shown in Fig. 11, see Fig. 14*b*. The antenna carrier, made of PC/ABS material with 1 mm thickness, is specially designed for the proposed antenna concept. The carrier has an inner wall for the support of coupler and to keep the right distance between the coupler and element. Besides supporting the antenna structure, the carrier also protects these fragile antennas. In addition, teflon tape is used between the coupler and the element to avoid short circuit.

From the scattering parameter measurements in Fig. 16 it is seen that the entire Tx and Rx frequency range is covered using the TDCA tuning range 0.75 – 3.5 pF and 1 – 4.5 pF, respectively. The measurements show that isolation better than 28 dB is feasible between Tx and Rx antennas.

Table 2 presents the measured total efficiency of the antenna system. The measurements are made at three

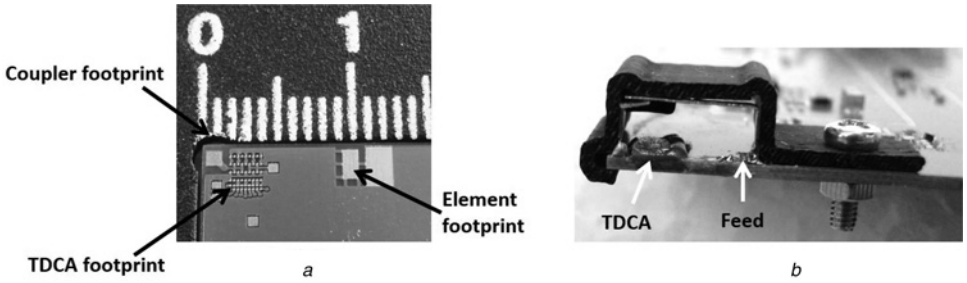

Fig. 14 *Tx antenna and its PCB layout*

a Footprint of antenna and TDCA
b Close-up of Tx antenna with carrier

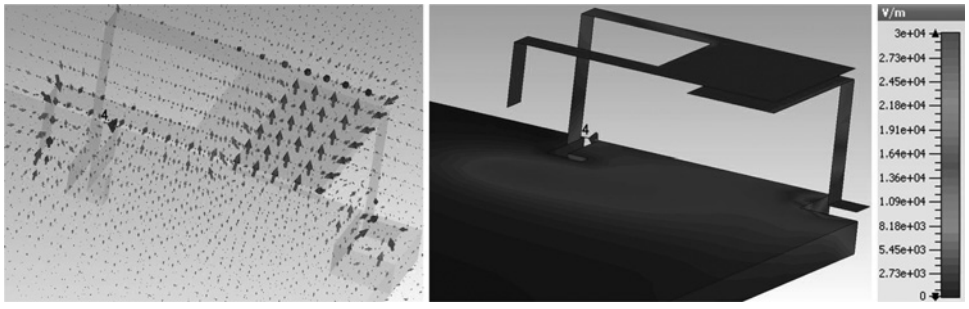

Fig. 15 *Electric field distribution*

doi: 10.1049/iet-smt.2014.0013

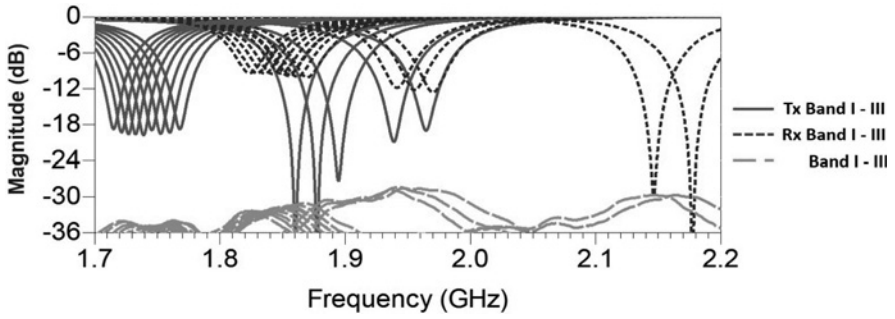

Fig. 16 *Measured scattering parameters*
Reflection coefficients (S_{11}, S_{22}) and coupling coefficient (S_{21}) of the Tx and Rx antennas

Table 2 Measured FS total efficiency with the carrier

	f_r, MHz	TDCA, pF	η_T, dB
Tx	1965	0.75	−2.1
	1830	1.5	−2.8
	1720	3.5	−4.0
Rx	2155	1.0	−2.4
	1945	2.25	−3.4
	1810	4.5	−4.4

different tuning states of the TDCA to obtain efficiency figures across the frequency range. The measured efficiency results are generally higher compared to simulated efficiency results from Table 1. This difference is mainly because of the addition of the carrier in measurements. Measurements with/without the carrier has shown that there is around 0.5 dB extra loss, at lowest tuning frequency, because of the carrier. The radiation properties of the antennas are depicted in Fig. 17, where omnidirectional characteristics are observed for both antennas.

5 Conclusions

High-Q antennas have higher imaginary (non-radiating) impedance, resulting in higher energy stored in electric and magnetic near-field components. Hence, they engender among other things, more losses in the tuning/matching components.

In this paper the aim is to design a very efficient high-Q reconfigurable antenna concept, that has either no or minimum number of physical matching components.

Therefore first a novel reconfigurable antenna concept design is presented for the unconventional FE, where the

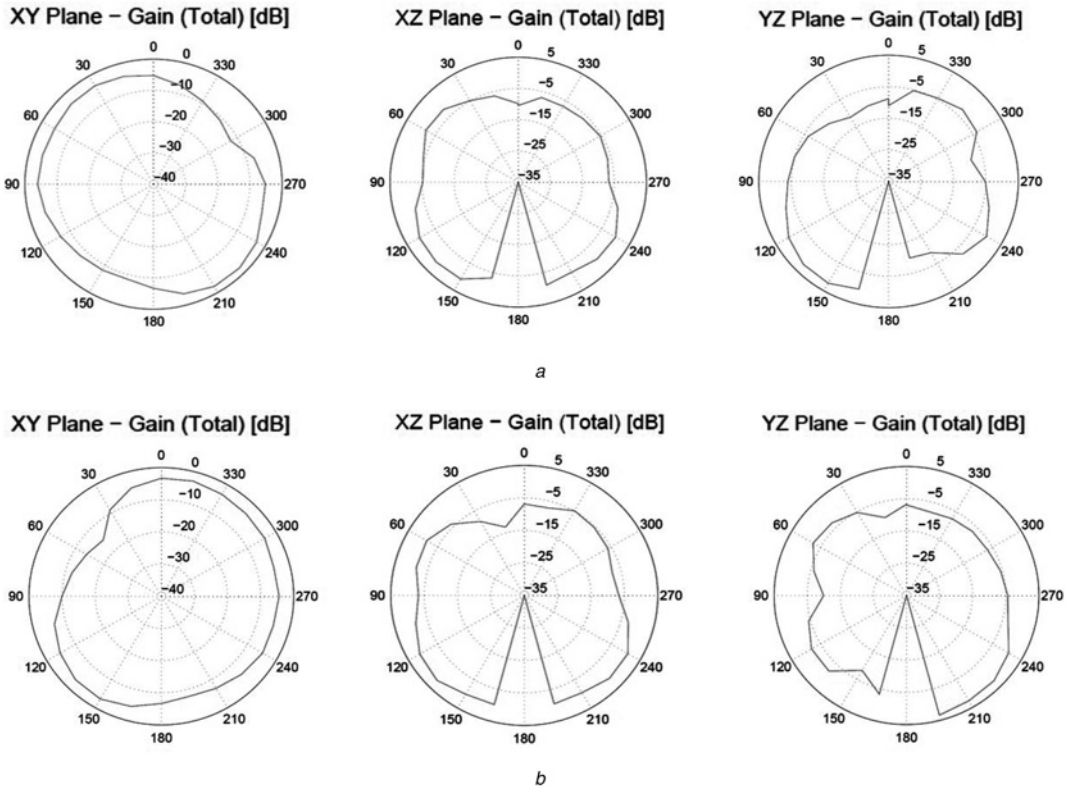

Fig. 17 *Measured radiation patterns (XY, XZ and YZ plane cuts)*
a Tx antenna at 1965 MHz
b Rx antenna at 2155 MHz

individual antennas cover half of the duplex for each corresponding frequency band, the transmitting and receiving half, respectively. It is shown that the antennas are able to cover the frequency range 1710–2170 MHz, and provide Tx–Rx filtering of more than 25 dB across the entire frequency range. In addition, the AC voltage across the tuning capacitor is shown to be decreasing as tuning down in frequency. Furthermore, the tuning resolution is simply controlled by adjusting the value of coupling capacitance, providing any required tuning resolution that fits the step size of the tunable capacitor.

Next, this antenna design is further improved by eliminating the physical matching components, leading to a self-matched antenna concept with only one physical component in use, which is the tunable capacitor. The self-matched antenna has around 1 dB better efficiency. In addition, the antenna exhibits robustness against ESD because the antenna element is shorted to ground and also because of the fact that the tuning capacitor C_t is not directly connected to the element.

Finally, the self-matched antennas are prototyped on fabricated PCB in order to verify the performance in measurements. The measurements show around 0.5 dB worse efficiency compared to simulations, which is mainly because of the addition of antenna carrier that was not presented in the simulations.

6 Acknowledgments

This work is supported by the Smart Antenna Front End (SAFE) project within the Danish National Advanced Technology Foundation – High Technology Platform.

7 References

1 Evolved Universal Terrestrial Radio Access (E-UTRA): User Equipment (UE) radio transmission and reception, 3GPP Std. TS 36.101, http://www.3gpp.org/ftp/Specs/html-info/36101.htm
2 Bhatti, R.A., Nguyen, N.A., Nguyen, V.A., Park, S.O.: 'Design of a compact internal antenna for multi-band personal communication handsets'. Presented at the APMC, Bangkok, Thailand, 2007
3 Wong, K.L.: 'Planar antennas for wireless communications', Microwave and Optical Engineering, (Wiley, New York, 2003), Ch. 2, pp. 26–69
4 Chiu, C.W., Lin, F.L.: 'Compact dual-band PIFA with multi-resonators', *Electron. Lett.*, 2002, **38**, (12), pp. 538–540
5 Wu, J., Panagamuwa, C.J., McEvoy, P., Vardaxoglou, J.C., Saraereh, O. A.: 'Switching a dual band PIFA to operate in four bands'. Proc. IEEE Antennas Propagation Soc. Int. Symp., 2006, pp. 2675–2678
6 Yoon, H.S., Park, S.O.: 'A new compact hexaband internal antenna of the planar inverted F-type for mobile handsets', *IEEE Antennas Wirel. Propag. Lett.*, 2007, **6**, pp. 336–339
7 Harrington, R.F.: 'Effect of antenna size on gain, bandwidth, and efficiency', *J. Res. Natl. Bur. Stand., Radio Propag.*, 1960, **64D**, (1), pp. 1–12
8 Alrabadi, O.N., Tatomirescu, A.D., Knudsen, M.B., Pelosi, M., Pedersen, G.F.: 'Breaking the transmitter-receiver isolation barrier in mobile handsets with spatial duplexing', *IEEE Trans. Antennas Propag.*, 2013, **61**, (4), pp. 2241–2251
9 Pelosi, M., Knudsen, M.B., Pedersen, G.F.: 'Multiple antenna systems with inherently decoupled radiators', *IEEE Trans. Antennas Propag.*, 2012, **60**, (2), pp. 503–515
10 Pelosi, M., Pedersen, G.F.: 'Future vogues in handset antenna systems'. IEEE Vehicular Technology Conf., 2011
11 Barrio, S.C.D., Tatomirescu, A., Pedersen, G.F., Morris, A.: 'Novel architecture for LTE world-phones', *IEEE Antennas Wirel. Propag. Lett.*, 2013, **12**, pp. 1676–1679
12 James, A.: 'Reconfigurable antennas for portable wireless devices', *IEEE Antennas Propag. Mag.*, 2003, **45**, (6), pp. 148–154
13 Tatomirescu, A., Alrabadi, O., Pedersen, G.F.: 'Tx-Rx isolation exploiting tunable balanced – unbalanced antennas architecture'. Loughborough Antennas and Propagation Conf., 12–13 November 2012
14 Pelosi, M., Alrabadi, O.N., Franek, O., Pedersen, G.F.: 'A novel figure of merit for small multiantenna systems: the duplex isolation'. Antennas and Propagation Society Int. Symp. (APSURSI), 2012
15 Barrio, S.C.D., Pelosi, M., Franek, O., Pedersen, G.F.: 'On the currents magnitude of a tunable planar-inverted-F antenna for low-band frequencies'. Sixth European Conf. EuCAP 2012, 2012
16 Barrio, S.C.D., Pedersen, G.F.: 'On the efficiency of capacitively loaded frequency reconfigurable antennas', *Int. J. Distrib. Sensor Netw.*, 2013, **2013**, Article ID 232909 (8p), doi:10.1155/2013/232909
17 Barrio, S.C.D., Pelosi, M., Pedersen, G.F.: 'On the efficiency of frequency reconfigurable high-Q antennas for 4G standards', *Electron. Lett.*, 2012, **48**, (16), pp. 982–983
18 Barrio, S.C.D., Pelosi, M., Franek, O., Pedersen, G.F.: 'The effect of the users body on high-Q and low-Q planar inverted F antennas for LTE frequencies'. IEEE 75th Vehicular Technology Conf. (VTC Spring), 2012, 2012
19 De Luis, J.R., Morris III, A., Gu, Q., de Flaviis, F.: 'Tunable duplexing antenna system for wireless transceivers', *IEEE Trans. Antennas Propag.*, 2012, **60**, (11), pp. 5484–5487
20 Nguyen, V.A., Ahmad, R., Park, S.O.: 'A simple PIFA based tunable internal antenna for personal communication handsets', *IEEE Antennas Wirel. Propag. Lett.*, 2008, **7**, pp. 130–133
21 Arrieta, C.R., de Haro, L.: 'Experiences on tuned multiband fractal antennas'. Proc. IEEE Antennas and Propagation Soc. Int. Symp., July 2005, vol. 2B, pp. 593–596
22 Nikolaou, S., Lugo, B.R., Carrasquillo, C., *et al.*: 'Pattern and frequency reconfigurable annular slot antenna using PIN diodes', *IEEE Trans. Antennas Propag.*, 2006, **54**, (2), pt. 1, pp. 439–448
23 Panayi, P.K., Al-Nuaimi, M.O., Ivrissimtzis, I.P.: 'Tuning techniques for planar inverted-F antenna', *Electron. Lett.*, 2001, **37**, (16), pp. 1003–1004
24 Bhartia, P., Bahl, I.J.: 'Frequency agile microstrip antennas', *Microw. J.*, 1982, **25**, pp. 67–70
25 Behdad, N., Sarabandi, K.: 'A varactor-tuned dual-band slot antenna', *IEEE Trans. Antennas Propag.*, 2006, **54**, pp. 401–408
26 Behdad, N., Sarabandi, K.: 'Dual-band recongurable antenna with a very wide tunability range', *IEEE Trans. Antennas Propag.*, 2006, **54**, (2), pp. 409–416
27 Nguyen, V., Dao, M., Lim, Y.T., Park, S.: 'A compact tunable internal antenna for personal communication handsets', *IEEE Antennas Wirel. Propag. Lett.*, 2008, **7**, pp. 569–572
28 Kawasaki, S., Itoh, T.: 'A slot antenna with electronically tunable length'. Antennas and Propagation Society Int. Symp., 1991. AP-S. Digest, 24–28 June 1991, vol. 1, pp. 130–133
29 Ollikainen, J., Kivekas, O., Vainikainen, P.: 'Low-loss tuning circuits for frequency-tunable small resonant antennas'. Symp. on Personal, Indoor and Mobile Radio Communications, 15–18 September 2002, vol. 4, pp. 1882–1887
30 Valkonen, R., Holopainen, J., Icheln, C., Vainikainen, P.: 'Broadband tuning of mobile terminal antennas'. Second European Conf. on Antennas and Propagation, 2007. EuCAP 2007, 11–16 November 2007, pp. 1–6
31 CST – Computer Simulation Technology. Available: www.cst.com
32 Advance Design System, Agilent Technologies, http://edocs.soco.agilent.com/display/doc/Home
33 Barrio, S.C.D., Pelosi, M., Pedersen, G.F., Morris, A.: 'Challenges for frequency-reconfigurable antennas in small terminals'. 2012 IEEE Vehicular Technology Conf. (VTC fall), 2012
34 Wispry Inc.: Tunable RF Solutions, 20 Fairbanks, Suite 198, Irvine, CA, 92618. Available: www.wispry.com